Phase Diagram of K_{x}Fe_{2-y}Se_{2-z}S_{z} and the Suppression of its Superconducting State by an Fe2-Se/S Tetrahedron Distortion

Hechang Lei (□□□), Milinda Abeykoon, Emil S. Bozin, Kefeng Wang (□□□), J. B. Warren, and C. Petrovic

Phys. Rev. Lett. **107**, 137002 — Published 19 September 2011

DOI: 10.1103/PhysRevLett.107.137002

Superconductivity in $K_xFe_{2-y}Se_{2-z}S_z$ ($0 \leqslant z \leqslant 2$) and Lattice Distortion

Hechang Lei (雷和畅),[1] Milinda Abeykoon,[1] Emil S. Bozin,[1] Kefeng Wang (王克锋),[1] J. B. Warren,[2] and C. Petrovic[1]
[1] *Condensed Matter Physics and Materials Science Department, Brookhaven National Laboratory, Upton, New York 11973, USA*
[2] *Instrumentation Division, Brookhaven National Laboratory, Upton, New York 11973, USA*

We report structurally tuned superconductivity in $K_xFe_{2-y}Se_{2-z}S_z$ ($0 \leqslant z \leqslant 2$) phase diagram. Superconducting T_c is suppressed as S is incorporated into the lattice, eventually vanishing at 80% of S. The magnetic and conductivity properties can be related to stoichiometry on poorly occupied Fe1 site and the local environment of nearly fully occupied Fe2 site. The decreasing T_c coincides with the increasing Fe1 occupancy and the overall increase in Fe stoichiometry from $z = 0$ to $z = 2$. Our results indicate that the irregularity of Fe2-Se/S tetrahedron is an important controlling parameter that can be used to tune the ground state in the new superconductor family.

PACS numbers: 74.62.Bf, 74.10.+v, 74.20.Mn, 74.70.Dd

The discovery of superconductivity in $K_xFe_{2-y}Se_2$ (AFeCh-122 type) with $T_c \approx 31$ K has triggered a renewed interest in the field of iron-based superconductors [1]. The crystal structure contains alkali metals and FeSe layers alternatively stacked along the c axis. When compared to other iron-based superconductors, AFeCh-122 show some distinctive features. Band structure calculations [2] and angle resolved photoemission spectroscopy (ARPES) measurements [3] indicate that the hole pockets are absent in AFeCh-122 system. This is different from other iron-based superconductors where both electron and hole Fermi surfaces (FSs) are present [4], suggesting that unconventional pairing via FS nesting [5],[6] might not be suitable for these materials. Experiments observed short and possibly long range magnetic order and its coexistence with superconductivity [7],[8],[9]. This is quite different from previous iron-based superconductors where superconductivity emerges when the spin density wave (SDW) state is suppressed [10]. Finally, the role of the ordered Fe vacancy and its relations to the magnetic order, metallic states and superconductivity remains unresolved.

Isovalent substitution is an effective way to study the relationship between structural parameters and physical properties. It is similar to pressure effects, because it should not change the carrier density. Unlike in the cuprates, superconductivity has been induced or enhanced by isovalent doping in iron-based superconductors, such as $BaFe_2(As_{1-x}P_x)_2$ and $FeTe_{1-x}Se_x$ [11],[12]. Recently, it was discovered that $K_xFe_{2-y}S_2$, isostructural to $K_xFe_{2-y}Se_2$, exhibits a spin glass (SG) semiconductor ground state without superconducting transition [13]. Here, we report the evolution of physical properties and structural parameters of $K_xFe_{2-y}Se_{2-z}S_z$ ($0 \leqslant z \leqslant 2$) single crystals. The results indicate that suppression of superconducting T_c coincides with the increasing occupancy of Fe on both Fe1 and Fe2 sites with S substitution, in contrast to $(Tl,K)_xFe_{2-y}Se_2$ [14]. It is found that the regularity of Fe2-Ch (Ch = Se, S) tetrahedron is an important controlling parameter for electronic and magnetic properties and has a major influence on electron pairing, i.e. on T_c.

Single crystals of $K_xFe_{2-y}Se_{2-z}S_z$ were grown as described previously [13],[15]. Powder X-ray diffraction (XRD) data were collected at 300 K using 0.3184 Å wavelength radiation (38.94 keV) at X7B beamline of the National Synchrotron Light Source. Refinements of the XRD data were performed using General Structure Analysis System (GSAS) [16],[17]. The average stoichiometry was determined by energy-dispersive x-ray spectroscopy (EDX) in a JEOL JSM-6500 scanning electron microscope. Electrical transport and magnetization measurements were carried out in Quantum Design PPMS-9 and MPMS-XL5.

XRD patterns of all $K_xFe_{2-y}Se_{2-z}S_z$ show (110) and other superlattice reflections associated with I4/m symmetry that incorporates Fe ordered vacancy site (Fig. 1(a)). The structure is shown in the inset of Fig. 1(b). The peak position of (110) shifts to higher angle with increasing S content, which indicates that lattice contracts gradually with S doping (Fig. 1(b) and Table 1), due to the smaller ionic size of S^{2-} than Se^{2-}. The trend of lattice contraction approximately follows the Vegard's law. The sum of Se and S stoichiometry in grown crystals is near 2.0, whereas both potassium and iron deviate from full occupancy (Table 1) [13],[15]. This is commonly found in all AFeCh-122 compounds [1],[13],[18]. It should be noted that the Fe content increases gradually with S doping, while the K content does not change monotonically. In addition, doping S into Se site does not lead to random Fe occupation of Fe1 and Fe2 sites. The refinements show that the Fe1 site is poorly occupied, whereas the Fe2 site is almost fully occupied.

The superconductivity of $K_xFe_{2-y}Se_{2-z}S_z$ single crystals with $z < 1.58$ is confirmed by the magnetization measurement (Fig. 2(a)). Zero-field-cooling (ZFC) superconducting transitions shift to low temperature with higher S content. Field-cooling (FC) susceptibilities are very small (Fig. 2(a)), implying possible strong vortex pinning. The most interesting feature in temperature de-

pendence of magnetization is the absence of Curie-Weiss law for all samples above 50 K as shown in Fig. 2(b) and (c) for H‖ab and H‖c, respectively. Magnetic susceptibilities are weakly temperature dependent with no significant anomalies above 50 K. This might suggest the presence of low dimensional short-range magnetic correlations and/or a long range antiferromagnetic (AFM) order above 300 K. This has been observed in $K_xFe_{2-y}Se_2$ crystals with different K and Fe sites occupancies [7],[9]. Therefore the magnetic interactions above 50 K are similar in the whole alloy series. On the other hand, non-superconducting samples show bifurcation between the ZFC and FC curves for both field orientations. The irreversible behavior suggests spin glass (SG) transition at low temperatures near $z = 2$ [13]. The spin glass freezing temperatures T_f for non-superconducting samples are determined from maximum position of $\chi_{ab}(T)$ in ZFC curves and listed in Table 1. The S-shape M(H) curves (Fig. 2(d)) at 1.8 K for $z = 1.58$ and $z = 2$ are similar [13],[19]. Hence, the SG state most likely persists in the $1.58 \leqslant z \leqslant 2$ range.

Besides $K_xFe_{2-y}S_2$, all other crystals show metallic behavior below a resistivity maximum $\rho_{\max}$ above superconducting transition (Fig. 3(a)). It should be noted that the temperature of $\rho_{\max}$ is not monotonic with the doping level of S (z), implying that the crossover may be influenced by the amount of both K and Fe deficiencies (Table 1). On the other hand, the crystal with $z = 2$ is semiconducting even if the Fe deficiency is smaller than in other samples. In contrast to $\rho_{\max}$, with the increase in S, the T_c is monotonically suppressed to lower temperature and can not be observed above 2 K for $z \geqslant 1.58$ (Table 1). We present the magnetic and superconducting phase diagram of $K_xFe_{2-y}Se_{2-z}S_z$ in Fig. 3(b). Semiconductor-metal crossover can be traced for $0 \leqslant z \leqslant 1.58$ at high temperature. In this region, $K_xFe_{2-y}Se_{2-z}S_z$ is a superconducting metal at low temperature. For $z = 1.58$, ρ(T) is metallic with no superconducting T_c down to 2 K. For $1.58 \leqslant z \leqslant 2$, we observe a drop in $\chi - T$ curves that could be related to a SG transition. For $z = 2$, the $K_xFe_{2-y}Se_{2-z}S_z$ becomes a small gap semiconductor with no metallic crossover and with a SG transition below 32 K.

The gradual changes of T_c are difficult to explain by the slight variation of Fe and K contents, because the T_c variation found with S doping is rather different from T_c variations due to K and Fe differences [14],[18],[20]. It was shown that the superconductivity appears with higher Fe content when K content (x) < 0.85 [18],[20]. As opposed to this trend, the $K_xFe_{2-y}Se_{2-z}S_z$ crystals with larger z values have higher Fe content but lower T_c.

Why is $K_xFe_{2-y}Se_2$ a superconductor whereas $K_xFe_{2-y}S_2$ is a semiconductor even though S is an isovalent substitution, similar to $FeTe_{1-x}Se_x$ [12]? This testifies that T_c is not only governed by K/Fe stoichiometry or vacancies. Below we show that superconductivity is in fact tuned by subtle structural effects induced by stoichiometry variation. The local environment of Fe profoundly changes with S, inducing the evolution of band structure and changes of physical properties. In the $K_xFe_{2-y}Se_{2-z}S_z$ crystal structure, Fe atoms have block-like distribution where every four Fe2 form a square around Se atom, making a cluster distinct from Fe1 site with low occupancy [21],[22]. Therefore there are Fe1-Fe2 distances as well as intra- and inter-cluster Fe2-Fe2 distances. The three types of distances are shown in Fig. 4(a). All cluster distances are unchanged with S doping whereas the Fe1-Fe2 distances decrease significantly (Fig. 4(a)). Similar magnetization behavior above 50 K and rather different superconducting T_c's as S content varies from 0 to 2 coincides with the nearly unchanged Fe2-Fe2 bond lengths. This shows that superconductivity is insensitive to the size of Fe2-Fe2 clusters whereas the unchanged high temperature magnetism could be related to the unchanged Fe2-Fe2 bond lengths. On the other hand, the SG behavior arising at the low temperature for non-superconducting samples can be explained by the non zero random occupancy of Fe1 (vacancy) site for higher S content (Fig. 4(b)), randomly changing the inter-cluster exchange interactions [23].

According to the empirical rule proposed by Mizuguchi et al., the critical temperature is closely correlated with the anion height between Fe and Pn (Ch) layers and there is an optimal distance (~ 1.38 $\mathring{A}$) with a maximum transition temperature $T_c \sim 55$ K [24]. This is invalid in $K_xFe_{2-y}Se_{2-z}S_z$ materials, where there are two Fe and two Ch sites and four Fe-Ch heights. This is because there is no monotonic decrease as T_c is tuned to 0 (Fig. 4(c)), whereas both Se and S end members have rather similar anion heights.

The bond angle α between Pn(Ch)-Fe-Pn(Ch) is another important factor since T_c in iron pnictides is optimized when Fe-Pn (Ch) tetrahedron is regular ($\alpha = 109.47°$) [25]. In $K_xFe_{2-y}Se_{2-z}S_z$, the Ch2-Fe1-Ch2 angle changes towards the optimal value with increasing S (Fig. 5(d)), but the local environment of Fe2 exhibits inverse trend. Among six angles in Fe2-Ch1(2) tetrahedron, three (Ch1-Fe2-Ch2) are nearly unchanged with S doping (Fig. 4(e)). The other three (Ch1-Fe2-Ch1) change significantly (maximum 6°) and deviate from optimal value from Se rich to S rich side (Fig. 4(f)). Hence, the increasing distortion of Fe2-Ch tetrahedron with S doping is closely correlated to the suppression of T_c. This distortion may lead to carrier localization, decreasing the density of states at the FS. Therefore, the regularity of Fe2-Ch1(2) tetrahedron is the key structural factor in the formation of the metallic states in $K_xFe_{2-y}Se_{2-z}S_z$, and consequently, the T_c. The dispersion of tetrahedral angles from 109.47° increases with S content increase.

We have demonstrated structure tuning of superconductivity in $K_xFe_{2-y}Se_{2-z}S_z$ single crystals. For low S doping, the superconducting T_c is nearly the same as in

the pure material. With the increase of S, above $z = 1$ the T_c is gradually suppressed finally vanishing at 80% of S substitution. Conductivity and magnetic properties coincide with stoichiometry changes on Fe1 site and with particular changes of the local environment of Fe2 site. Nearly unchanged Fe2-Fe2 bond lengths result in the similar magnetic behavior. The suppression of superconductivity with S doping could be traced to the increasing irregularity of Fe2-Ch tetrahedron and to increasing occupancy of Fe1 site. These ultimately destroy superconductivity and bring about glassy magnetic order and semiconducting ground state.

We thank Jonathan Hanson for help with XRD experiment. Work at Brookhaven is supported by the U.S. DOE under Contract No. DE-AC02-98CH10886 and in part by the Center for Emergent Superconductivity, an Energy Frontier Research Center funded by the U.S. DOE, Office for Basic Energy Science.

[1] J. Guo, S. Jin, G. Wang, S. Wang, K. Zhu, T. Zhou, M. He, and X. Chen, Phys. Rev. B **82**, 180520(R) (2010).
[2] I. R. Shein and A. L. Ivanovskii, Physics Letters A **375**, 1028 (2011).
[3] Y. Zhang, L. X. Yang, M. Xu, Z. R. Ye, F. Chen, C. He, J. Jiang, B. P. Xie, J. J. Ying, X. F. Wang, X. H. Chen, J. P. Hu, and D. L. Feng, Nat. Mater. **10**, 273 (2011).
[4] H. Ding, P. Richard, K. Nakayama, K. Sugawara, T. Arakane, Y. Sekiba, A. Takayama, S. Souma, T. Sato, T. Takahashi, Z. Wang, X. Dai, Z. Fang, G. F. Chen, J. L. Luo, and N. L. Wang, EPL **83**, 47001 (2008).
[5] I. I. Mazin, D. J. Singh, M. D. Johannes, and M. H. Du, Phys. Rev. Lett. **101**, 057003 (2008).
[6] K. Kuroki, S. Onari, R. Arita, H. Usui, Y. Tanaka, H. Kontani, and H. Aoki, Phys. Rev. Lett. **101**, 087004 (2008).
[7] D. A. Torchetti, M. Fu, D. C. Christensen, K. J. Nelson, T. Imai, H. C. Lei, and C. Petrovic, Phys. Rev. B **83**, 104508 (2011).
[8] V. Yu. Pomjakushin, D. V. Sheptyakov, E. V. Pomjakushina, A. Krzton-Maziopa, and K. Conder, D. Chernyshov and V. Svitlyk, and Z. Shermadini, Phys. Rev. B **83**, 144410 (2011).
[9] V. Yu. Pomjakushin, E. V. Pomjakushina, A. Krzton-Maziopa, K. Conder, and Z. Shermadini, J. Phys. Condens. Matter **23**, 156003 (2011).
[10] C. de la Cruz, Q. Huang, J. W. Lynn, J. Y. Li, W. Ratcliff II, J. L. Zarestky, H. A. Mook, G. F. Chen, J. L. Luo, N. L. Wang, and P. C. Dai, Nature **453,** 899 (2008).
[11] S. Jiang, H. Xing, G. F. Xuan, C. Wang, Z. Ren, C. M. Feng, J. H. Dai, Z. A. Xu, and G. H. Cao, J. Phys. Condens. Matter **21**, 382203 (2009).
[12] K.-W. Yeh, T. W. Huang, Y. L. Huang, T. K. Chen, F. C. Hsu, P. M. Wu, Y. C. Lee, Y. Y. Chu, C. L. Chen, J. Y. Luo, D. C. Yan, and M. K. Wu, EPL 84, 37002 (2008).
[13] H. C. Lei, M. Abeykoon, E. S. Bozin, and C. Petrovic, Phys. Rev. B **83**, 180503(R) (2011).
[14] M. H. Fang, H. D. Wang, C. H. Dong, Z. J. Li, C. M. Feng, J. Chen, and H. Q. Yuan, EPL **94**, 27009 (2011).
[15] H. C. Lei, and C. Petrovic, Phys. Rev. B **83**, 184504 (2011).
[16] A. C. Larson and R. B. Von Dreele, Los Alamos National Laboratory Report LAUR 86-748 (1994).
[17] B. H. Toby, J. Appl. Cryst. **34**, 210 (2001).
[18] D. M. Wang, J. B. He, T.-L. Xia, and G. F. Chen, Phys. Rev. B 83, 132502 (2011).
[19] J. J. Ying, A. F. Wang, Z. J. Xiang, X. G. Luo, R. H. Liu, X. F. Wang, Y. J. Yan, M. Zhang, G. J. Ye, P. Cheng and X. H. Chen, arXiv:1012.2929.
[20] Y. J. Yan, M. Zhang, A. F. Wang, J. J. Ying, Z. Y. Li, W. Qin, X. G. Luo, J. Q. Li, J. P. Hu, and X. H. Chen, arXiv:1104.4941 (2011).
[21] W.-G. Yin, C.-H. Lin, and W. Ku, arxiv: 1106.0881 (2011).
[22] W. Bao, G. N. Li, Q. Huang, G. F. Chen, J. B. He, M. A. Green, Y. Qiu, D. M. Wang, and J. L. Luo, arxiv: 1102.3674 (2011).
[23] M. Oledzka, K. V. Ramanujachary, and M. Greenblatt, Mater. Res. Bull. **31,** 1491 (1996).
[24] Y. Mizuguchi, Y. Hara, K. Deguchi, S. Tsuda, T. Yamaguchi, K. Takeda, H. Kotegawa, H. Tou, and Y. Takano, Supercond. Sci. Technol. **23,** 054013 (2010).
[25] C.-H. Lee, A. Iyo, H. Eisaki, H. Kito, M. T. Fernandez-Diaz, T. Ito, K. Kihou, H. Matsuhata, M. Braden, and K. Yamada, J. Phys. Soc. Jap., 77, 083704 (2008).

FIGURES

FIG. 1. (a) Powder XRD patterns of $K_xFe_{2-y}Se_{2-z}S_z$ at 300 K and fit using I4/m space group. Inset: (110) peak position with different S content. (b) Unit cell parameters as a function of S substitution. Inset: Crystal structure of $K_xFe_{2-y}Se_{2-z}S_z$ in I4/m unit cell with vacant Fe1 sites marked light red and Fe2 sites marked dark purple.

FIG. 2. (a) dc magnetic susceptibility of superconducting $K_xFe_{2-y}Se_{2-z}S_z$ samples below 35 K at H = 10 Oe for H$\|$ab in ZFC and FC. (b) and (c) Temperature dependence of χ(T) of $K_xFe_{2-y}Se_{2-z}S_z$ at H = 1 kOe for H$\|$ab and H$\|$c in ZFC and FC, respectively. (d) M-H loops of non-superconducting samples at 1.8 K for H$\|$c.

FIG. 3. (a) Temperature dependence of the in-plane resistivity $\rho_{ab}(T)$ of the $K_xFe_{2-y}Se_{2-z}S_z$ single crystals in zero field. Inset: temperature dependence of $\rho_{ab}(T)$ below 40 K for $0 \leqslant z \leqslant 1.2$. (b) Magnetic and superconducting phase diagram of $K_xFe_{2-y}Se_{2-z}S_z$. Green, blue and orange colors show semiconducting, magnetic and superconducting regions, respectively. Red symbols denote spin glass transitions.

FIG. 4. (a) Bond lengths between Fe1(2) and Fe1(2). Inset shows top view of Fe layer. (b) Occupancy of Fe1 and Fe2. (c) Anion height. Inset shows side view of Fe-Ch sheet. (d) Ch2-Fe1-Ch2, (e) Ch1-Fe2-Ch2, and (f) Ch2-Fe2-Ch2 bond angles of $K_xFe_{2-y}Se_{2-z}S_z$ as a function of S substitution, x. Insets of (d)-(f) show Fe-Ch tetrahedron for Fe1-Ch1 and Fe2-Ch1(2). The dotted pink line in (c) shows the optimal bond lengths for T_c. The dotted green lines in (d)-(f) indicate the optimal angle for T_c.

TABLES

TABLE I. Structural, magnetic and transport properties of $K_xFe_{2-y}Se_{2-z}S_z$. T_f is determined from maximum position of $\chi_{ab}(T)$ in zero-field-cooling curve. $T_{\rho_{max}}$, $T_{c,onset}$ and $T_{c,0}$ are obtained from resistivity data. Error bars for T_c, T_f, and $T_{\rho_{max}}$ reflect standard deviation from the average temperatures measured on several crystals grown in one batch.

$K_xFe_{2-y}Se_{2-z}S_z$	a (Å)	c (Å)	$T_{c,onset}$ (K)	$T_{c,0}$ (K)	T_f (K)	$T_{\rho_{max}}$ (K)
$K_{0.64(4)}Fe_{1.44(4)}Se_{2.00(0)}$	3.911(2)	14.075(3)	33(1)	31(1)		132(6)
$K_{0.73(3)}Fe_{1.44(3)}Se_{1.68(6)}S_{0.32(5)}$	3.847(2)	14.046(4)	33(1)	31(1)		129(4)
$K_{0.70(7)}Fe_{1.55(7)}Se_{1.01(2)}S_{0.99(2)}$	3.805(2)	13.903(6)	24(2)	21(1)		203(20)
$K_{0.76(5)}Fe_{1.61(5)}Se_{0.96(4)}S_{1.04(5)}$	3.797(2)	13.859(3)	18(1)	16(2)		138(5)
$K_{0.80(8)}Fe_{1.64(8)}Se_{0.42(5)}S_{1.58(0.05)}$	3.781(2)	13.707(2)			17(1)	79(14)
$K_{0.80(1)}Fe_{1.72(1)}S_{2.00(1)}$	3.753(2)	13.569(3)			32(1)	

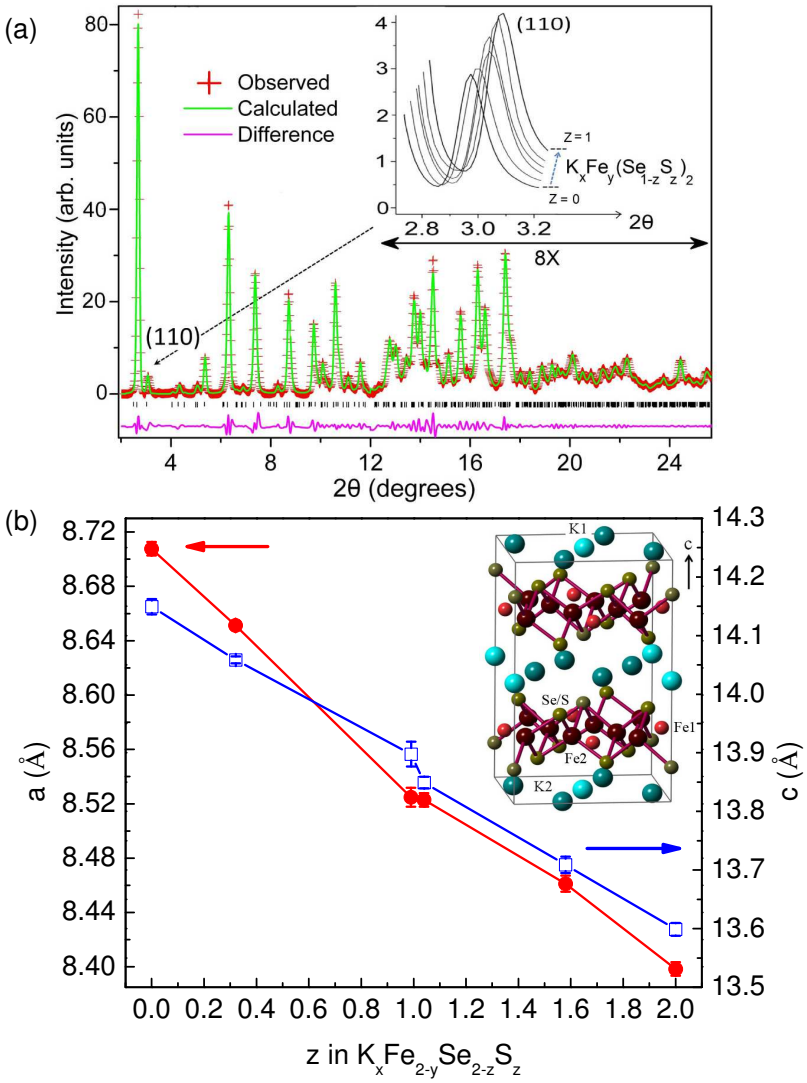

Figure 1 LF13705 27Jul2011

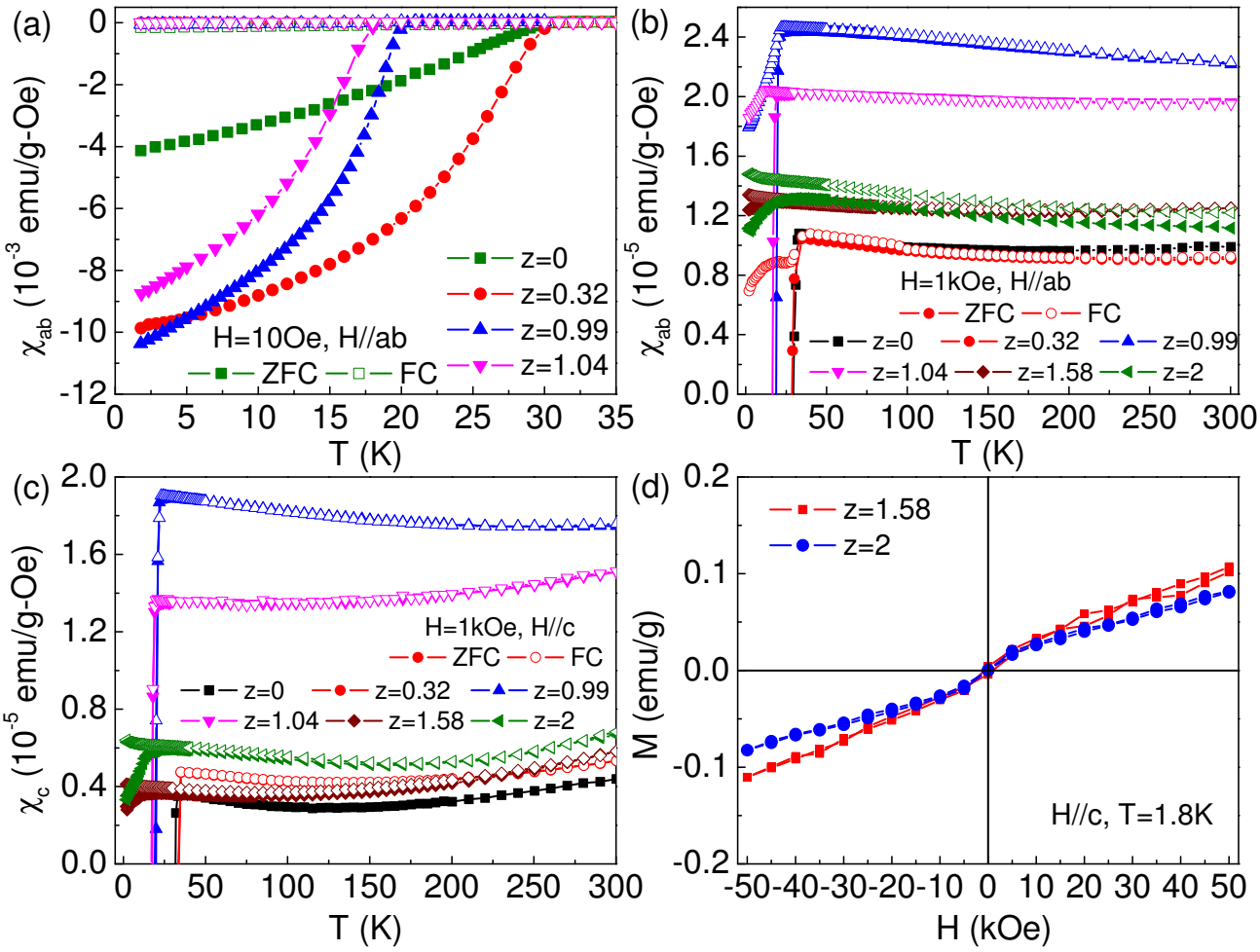

Figure 2 LF13705 27Jul2011

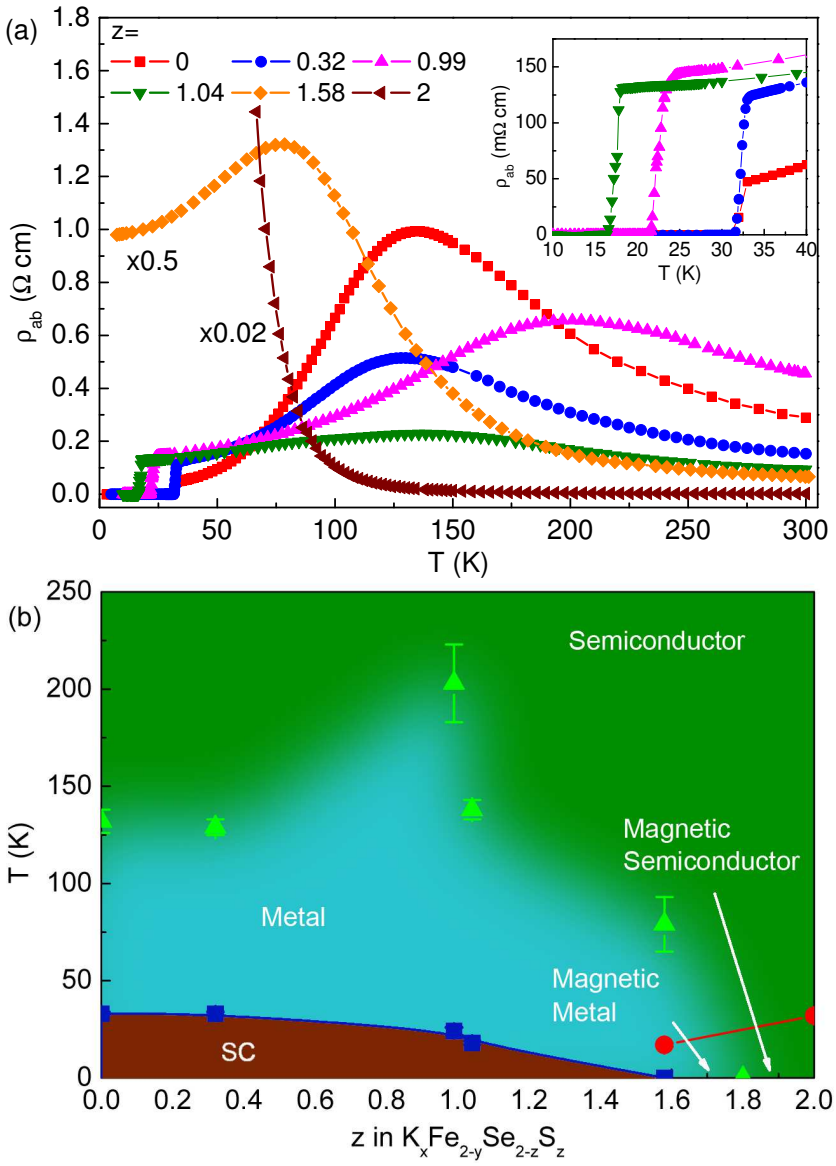

Figure 3 LF13705 27Jul2011

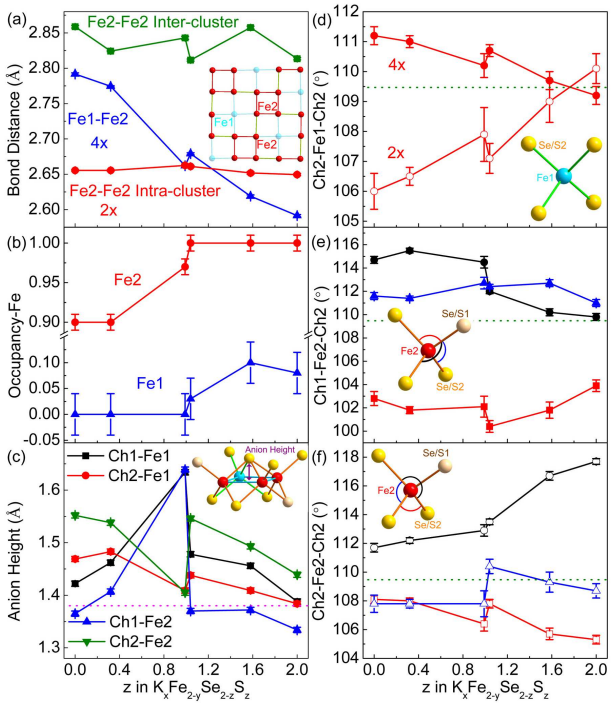

Figure 4 LF13705 27Jul2011